Localization of an excess electron in water clusters[a)]

A. Wallqvist, D. Thirumalai,[b)] and B. J. Berne
Department of Chemistry, Columbia University, New York, New York 10027

(Received 11 November 1985; accepted 24 April 1986)

Simulation of e^-–$(H_2O)_n$ for $n = 1,2,3$ done at 5 K, using path integral Monte Carlo methods shows that a water dimer as well as a water trimer in the linear configuration can bind an electron in a diffuse surface state. The binding energy of the electron dimer and the electron trimer is estimated to be between 3–6 and 4–9 meV, respectively. The results indicate that the electron does not alter the structure of the water dimer but does induce observable changes in the water trimer. It is also shown that an electron does not bind to a monomer. These results are discussed in connection with recent molecular beam experiments.

I. INTRODUCTION

The structure of the solvated electron continues to be of considerable theoretical and experimental interest.[1–4] An excess electron in a fluid may be free, quasifree, weakly localized, or strongly localized depending on the nature of the solvent, the density, and the temperature.[5] The nature of electron states in a wide variety of media has been investigated both experimentally and theoretically.[6–10] Many of the models that have been used to predict the structural and dynamical properties of the electron in polar solvents have been purely phenomenological in nature.[11] Ignorance of the effect of short and long range forces felt by an electron in a fluid environment has forced investigators to use very crude models.[12] Recent *ab initio* studies of the stability of an electron in clusters are thus very useful.[13–18] By performing these calculations as a function of the number of molecules in the cluster one can develop a model-independent understanding of the forces operative in a medium.

The study of a localized electron in clusters is important in a variety of physical situations such as (a) in understanding the formation of electronic surface or bulk states, (b) in the theories of electron attachment, and (c) as a model for the theoretical description of electron transfer processes in condensed matter. There is a more direct reason to explore the nature of the binding of an electron to water clusters. Haberland *et al.* have recently examined the stability of e^-–$(H_2O)_n$ systems as a function of n, the number of water molecules comprising a cluster, in molecular beam experiments.[19] They showed that the e^-–$(H_2O)_n$ system is stable when $n \geqslant 11$. More surprisingly,[20] when the beam is seeded with Ar atoms to effectively lower the beam temperature, two water molecules can localize an electron. They find that e^-–$(H_2O)_n$ is not stable for $n = 3$, 4, or 5. Interestingly, before these experimental results were published all previous attempts to observe negatively charged water clusters were unsuccessful.[21] Spurred by these findings, and given the obvious importance of thoroughly understanding the nature of the hydrated electron, we have begun to explore the stability and structure of an electron interacting with water clusters. Our calculations are based on pseudo potentials. Path integral Monte Carlo methods are then used to investigate the possibility of electron localization in water clusters as a function of the cluster size. This method is probably not as accurate as *ab initio* calculations but has the advantage of being applicable to larger clusters. Model potentials that describe the energetics of electron–water clusters fairly accurately can then be used in quantum mechanical simulations of an electron in liquid water.[22,23] In this article we report our results for the stability and structure of e^-–$(H_2O)_n$ system for $n = 1$, 2, and 3 using path integral Monte Carlo (PIMC) techniques.

II. METHODOLOGY

The path integral Monte Carlo method is used to simulate an electron interacting with N water molecules. The Hamiltonian for the system is given by

$$H = \frac{\mathbf{p}^2}{2m} + \sum_{i=1}^{N} \sum_{\alpha=1}^{3} \frac{\mathbf{P}_{i(\alpha)}^2}{2M_\alpha} + \sum_{i>j}^{N} V(\mathbf{R}_i,\mathbf{R}_j) + \sum_{i=1}^{N} U(\mathbf{r},\mathbf{R}_i), \tag{1}$$

where $\mathbf{R}_i$ denotes the collection of coordinates of the ith water molecule, $\mathbf{r}$ is the location of the excess electron, $\mathbf{p}$ is the momentum conjugate to $\mathbf{r}$, m is the mass of the electron, M_α is the mass of the αth species (H, H, and O) in a water molecule, $P_{i(\alpha)}$ is the momentum of the αth species, $V(\mathbf{R}_i,\mathbf{R}_j)$ is the interaction potential between two water molecules, and $U(\mathbf{r},\mathbf{R}_i)$ is the interaction potential of the electron and the ith water molecule. The term $V(\mathbf{R}_i,\mathbf{R}_j)$ is taken to be the modified central force potential of water.[24] The internal vibrations of the water molecule are modeled by a set of Morse potentials.[25] This was precisely the model for the water–water interaction used in the recent path integral simulation of small clusters of water molecules as well as pure water.[26]

In this paper we assume that the electron–water monomer interaction, $U^1(\mathbf{r},\mathbf{R}_i)$, consists of three parts: (a) an exponential repulsive interaction due to the closed shell water electrons. This term is also designed to mimic the constraint that the orbitals of the excess electron be orthogonal to those of the bound electrons. This is in the same spirit as the construction of the effective core potentials[27]; (b) an

[a)] Supported in part by grants from the National Science Foundation and the National Institutes of Health.

[b)] Present address: Institute for Physical Science and Technology and Department of Chemistry and Biochemistry, University of Maryland, College Park, MD 20742.

 0021-9606/86/151583-09$02.10

anisotropic electron–dipole interaction centered on the center of charge of H_2O; and (c) an electron-induced dipole interaction due to the water polarizability centered on the oxygen atom. Parts (b) and (c) contain a switching function which turns off these interactions when the electron gets close to the respective centers. In this model the electron is not allowed to penetrate the surface of the water molecule which is justified for the very low energy electrons considered here. The functional form for the first model potential $U^{\mathrm{I}}(\mathbf{r},\mathbf{R}_i)$ is given by

$$U^{\mathrm{I}}(\mathbf{r},\mathbf{R}_i) = -\frac{e\mu}{|\mathbf{r}_{eCD}^{(i)}|^2}\left[\frac{(\mathbf{R}_{CD}^{(i)}-\mathbf{R}_O^{(i)})\cdot(\mathbf{r}-\mathbf{R}_{CD}^{(i)})}{|\mathbf{R}_{CD}^{(i)}-\mathbf{R}_O^{(i)}||\mathbf{r}-\mathbf{R}_{CD}^{(i)}|}\right] S(|\mathbf{r}_{eCD}^{(i)}|) - \frac{\alpha_O}{2r_{eO}^4} S(|\mathbf{r}_{eO}^{(i)}|) + V_0 e^{-|\mathbf{r}_{eO}^{(i)}|/r_{OH}^{eq}}, \tag{2}$$

where the switching function $S(|\mathbf{r}|)$ is taken to be

$$S(r) = 1 - \exp(-r/r_c)^{12}, \tag{3}$$

with r_c, the cut-off distance, was set equal to the equilibrium oxygen–hydrogen bond distance. The vector positions are defined as follows:

$$\mathbf{R}_{CD}^{(i)} = \tfrac{1}{4}(\mathbf{R}_{H_1}^{(i)} + \mathbf{R}_{H_2}^{(i)} - 2\mathbf{R}_O^{(i)}) + \mathbf{R}_O^{(i)}, \tag{4a}$$

$$\mathbf{r}_{eCD}^{(i)} = \mathbf{r} - \mathbf{R}_{CD}^{(i)}, \tag{4b}$$

$$\mathbf{r}_{eO}^{(i)} = \mathbf{r} - \mathbf{R}_O^{(i)}. \tag{4c}$$

In Eq. (4) $\mathbf{R}_{CD}^{(i)}$ is the center of the dipole of the ith water molecule, $\mathbf{r}_{eCD}^{(i)}$ is the vector distance between the electron and the center of charge $\mathbf{R}_{CD}^{(i)}$, $\mathbf{R}_O^{(i)}$ is the position of the ith oxygen atom and $\mathbf{r}_{eO}^{(i)}$ is the distance between the oxygen atom of the ith water molecule and the electron.

In Eq. (2) μ is the dipole moment of the isolated water molecule, α_O is the spherical dipole polarizability, V_0 is the strength of the short range repulsion, and r_{OH}^{eq} is the equilibrium oxygen–hydrogen distance in an isolated water molecule. The values of μ, α_O,[28] V_0 and r_{OH}^{eq} are taken to be 1.84 D, 1.45 Å^3, 21.754 eV, and 0.96 Å, respectively. In order to assess the importance of the spherical dipole polarizability we constructed another model potential omitting the second term in $U^{\mathrm{I}}(\mathbf{r},\mathbf{R}_i)$. The strength of the repulsive term and the distance at which the charge-dipole term was switched off were suitably modified. In particular the value of V_0 is changed to 18.128 eV. The resulting potential will be referred to as $U^{\mathrm{II}}(\mathbf{r},\mathbf{R}_i)$. The accuracy of our model potentials can be assessed by comparing our results to *ab initio* calculations as shown below.

Figure 1 shows how $U^{\mathrm{I}}(\mathbf{r},\mathbf{R}_i)$ and $U^{\mathrm{II}}(\mathbf{r},\mathbf{R}_i)$ depend on r for the case when the electron approaches the center of the dipole R_{CD}, along the dipole direction. $U^{\mathrm{I}}(\mathbf{r},\mathbf{R}_i)$ exhibits an asymmetric double well character for $0.7 < r < 1.6$ Å. This is due to the different switching functions used for the charge-dipole and spherical polarizability terms in the potential and therefore has no physical significance. $U^{\mathrm{II}}(\mathbf{r},\mathbf{R}_i)$, which does not include the spherical polarizability term, has a single minimum at $r = 1.38$ Å and the well depth is about 338 meV. The well depth corresponding to the deeper of the two

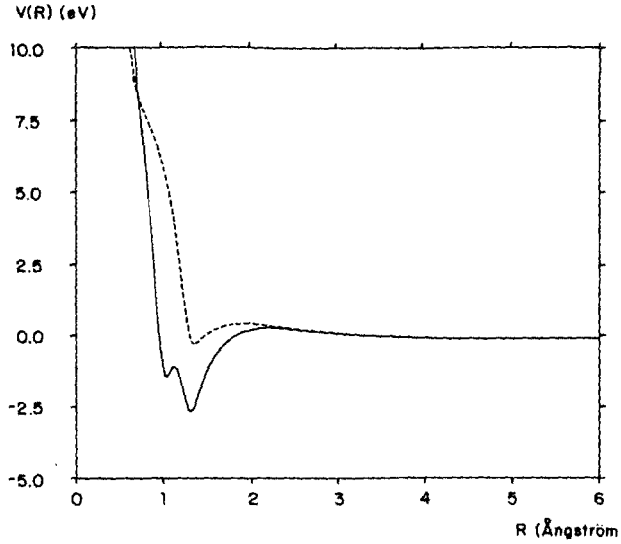

FIG. 1. The electron–water monomer potential (in eV) as a function of r (in angstroms) when the electron approaches the center of dipole R_{CD} along the direction of the dipole, i.e., when $\mathbf{r}\cdot\mathbf{R}_{CD} = 1$. The solid line corresponds to $U^{\mathrm{I}}(\mathbf{r},\mathbf{R}_i)$ and the dotted line corresponds to $U^{\mathrm{II}}(\mathbf{r},\mathbf{R}_i)$. The functional form for $U^{\mathrm{I}}(\mathbf{r},\mathbf{R}_i)$ is displayed in the text [cf. Eq. (2)].

minima of $U^{\mathrm{I}}(\mathbf{r},\mathbf{R}_i)$ is a factor of 7.8 larger and is therefore expected to induce stronger localization. It is interesting to observe that both these model potentials have a wide barrier extending from 1.5–3.0 Å. The barrier height for $U^{\mathrm{I}}(\mathbf{r},\mathbf{R}_i)$ is 229.1 meV whereas it is 356.9 meV for $U^{\mathrm{II}}(\mathbf{r},\mathbf{R}_i)$. Because the potential is anisotropic these quantities depend on the direction of approach of the electron. The presence of the barrier, which is quite central to the physics of localization in these systems, is also found in the recent Hartree–Fock calculations of the electron water potential.[29]

For a given Hamiltonian and a specified temperature T we can calculate all the equilibrium properties of the system from the canonical partition function Q which is given by

$$Q = \mathrm{Tr}(e^{-\beta H/P})^P,$$

where $\beta = 1/kT$. If P is very large then using the discretized path integral formulation Q can be conveniently written as[7,30]

$$Q_p = \left(\frac{mP}{2\pi\hbar^2\beta}\right)^{3P/2}\left(\frac{M_OP}{2\pi\hbar^2\beta}\right)^{3NP/2}\left(\frac{M_HP}{2\pi\hbar^2\beta}\right)^{3NP} \times \int \exp(-S_{\mathrm{eff}}) \prod_{i=1}^{N}\prod_{j=1}^{P} d\mathbf{R}_i^{(j)}\, d\mathbf{r}^{(j)}, \tag{5}$$

$$S_{\mathrm{eff}} = \beta(V_{e\text{-}w} - V_{w\text{-}w}), \tag{6a}$$

with

$$V_{e\text{-}w} = \sum_{j=1}^{P}\left[\frac{mP}{2\hbar^2\beta^2}(\mathbf{r}^{(j)} - \mathbf{r}^{(j+1)})^2 + \frac{1}{P}\sum_{i=1}^{N} V(\mathbf{r}^{(j)},\mathbf{R}_i^{(j)})\right] \tag{6b}$$

and

$$V_{w\text{-}w} = \sum_{i=1}^{N}\left[\sum_{j=1}^{P}\sum_{\alpha=1}^{3}\frac{M_\alpha P}{2\hbar^2\beta^2}(\mathbf{R}_{i(\alpha)}^{(j)} - \mathbf{R}_{i(\alpha)}^{(j+1)})^2 + \frac{1}{2P}\sum_{k=1}^{N} V(\mathbf{R}_i^{(j)},\mathbf{R}_k^{(j)})\right]. \tag{6c}$$

Thus in the discretized path integral formulation the system consisting of $3N + 1$ quantum particles is isomorphic to $3NP + P$ classical particles moving in a potential field given by Eq. (6). The formulation allows us to evaluate Q and all the relevant properties (like energy, distribution functions) by classical Monte Carlo techniques.

Starting from an arbitrary initial configuration the isomorphic classical system was equilibrated. To accelerate the equilibration process the number of equivalent pseudoparticles P was increased slowly from a small number to the final desired value. The calculations reported in this paper were done with the number of particles in the electron chain equal to $P = 1000$ and the number of beads in the hydrogen and oxygen chains set to 100. After the system equilibrated, the results reported here were obtained by averaging over the subsequent 13 000 passes. Our simulations employed two types of moves, the displacement of each bead on a given ring polymer and the translation of the center of mass of the ring polymer. In addition, for the water molecules, a third type of move involving the translation of the center of mass of the entire chain representing the water molecule was made. The acceptance ratios for all the moves were chosen to be between 0.3–0.5 except that for the translation of the electron ring polymer where the acceptance probability was adjusted to be between 0.6–0.7. The criteria for binding is determined by (a) the overall external potential energy between the electron and water clusters, (b) the behavior of the external electron oxygen radial distribution function $g_{eO}(r)$, and (c) examination of the configuration of the $e^-(H_2O)_n$ system. The nature of the electron state is inferred by inspecting the configurations generated during the calculation. We should emphasize that the results reported here are independent of the step size used in the Monte Carlo simulation. Unless otherwise stated all the calculations were done at 5 K.

III. RESULTS AND DISCUSSION

A. Electron–water monomer

The initial configuration for the electron monomer was obtained by removing a water molecule from the $e^-(H_2O)_2$ system (discussed below). The binding energy of the electron–monomer is so small that we cannot distinguish it from zero. The electron–oxygen radial distribution functions $g^{I}_{eO}(r)$ and $g^{II}_{eO}(r)$ corresponding to the model potentials $U^{I}(\mathbf{r},\mathbf{R}_i)$ and $U^{II}(\mathbf{r},\mathbf{R}_i)$, respectively, exhibit a flat region from $r \sim 1$ Å onward indicating that the electron is essentially free of the monomer. The configuration of the electron–monomer system generated during the calculation shows that the electron chain physically separates from the water molecule. This is not surprising since the dipole moment of the water molecule is less than the critical value needed to localize an electron.[31] The *ab initio* calculations of Chipman also suggested that a water monomer in its equilibrium configuration cannot bind an electron. He did find, however, that in some unusually distorted geometries—geometries of H_2O not accessible in beam experiments—the binding energy can be as high as 3.75 meV.

B. Electron–water dimer

Several sets of initial starting configurations were employed. In almost all cases the water molecules were initially close together. This was partly inspired by Chipman's[14] observations that the geometry of the water dimer in the presence of the electron is very similar to that of the neutral dimer. However, in order to study other geometries initial configurations with the two water dipoles pointing in opposite directions were employed. The water molecules rapidly reoriented to form a hydrogen bond as in the neutral equilibrium water dimer. The results reported here were independent of the several starting configurations.

The water dimer energies remain essentially unchanged in the presence of the excess electron. The binding energy, which is taken to be the average potential energy between the electron and the water dimer, is found to be about 3–6 meV using $U^{I}(\mathbf{r},\mathbf{R}_i)$. The binding energy using $U^{II}(\mathbf{r},\mathbf{R}_i)$ is lowered to about 2–3 meV. These values are in good agreement with the LCAO-MO-SCF calculations of Chipman,[14] who estimated that the binding energy is between 0.2 and 9 meV depending on the water dimer geometry. Figure 2 shows the electron–oxygen pair correlation functions, $g^{I}_{eO}(r)$ and $g^{II}_{eO}(r)$ corresponding to model potentials I and II, respectively, as a function of r. The solid line representing $g^{I}_{eO}(r)$ exhibits two very narrow peaks at $r < 2.0$ Å. This corresponds to the electron density trapped in the asymmetric double well in $U^{I}(\mathbf{r},\mathbf{R}_i)$ when the electron approaches the water in the z direction (cf. Fig. 1). It is also seen that for $r > 2$ Å there is a peak in the density at around 9 Å followed by a slowly decaying tail with a range of about 30–40 Å. A qualitatively similar result is obtained when potential II is used with the exception that the two sharp peaks are missing, that is, there is no probability of finding the electron $r \leq 1$ Å. In addition the peak at $r \sim 9$ Å is less pronounced than seen in $g^{I}_{eO}(r)$ but the tail in $g^{II}_{eO}(r)$ also vanishes where the tail of $g^{I}_{eO}(r)$ does. Examination of the radial distribution of the oxygens around the electron barycenter $g_{e_{COM}O}(r)$ (not shown here) indicates that the center of mass of the electron chain is within 20–30 Å of the water dimer. These observa-

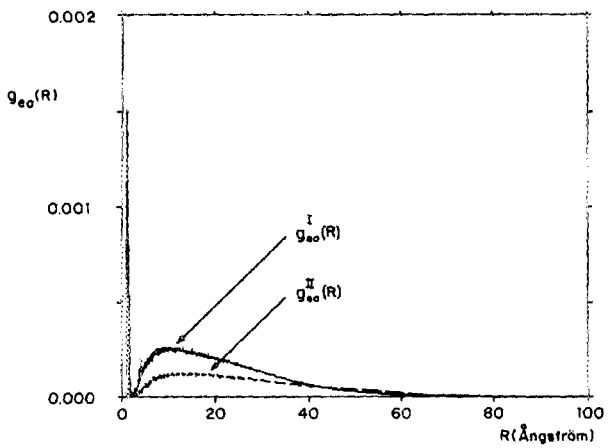

FIG. 2. Plot of the electron–oxygen radial distribution functions $g^{I}_{eO}(r)$ and $g^{II}_{eO}(r)$ as a functtion of r calculated using $U^{I}(\mathbf{r},\mathbf{R}_i)$ and $U^{II}(\mathbf{r},\mathbf{R}_i)$, respectively, for the electron–water dimer system.

tions clearly indicate that the bound electron resembles a very diffuse cloud. Comparison of the results obtained using the two model potentials I and II suggest that the inclusion of the polarizability not only lowers the energy of the localized state, but also alters the electron density distribution as depicted by the electron–oxygen radial distribution function. A closer examination of Fig. 2 indicates that there is a spike in $g^{\mathrm{I}}_{e\mathrm{O}}(r)$ at $r \sim 4$ Å. The bulk of the electron density is located around a single water molecule (which is more clearly demonstrated below) and the spike seen in $g^{\mathrm{I}}_{e\mathrm{O}}(r)$ corresponds to the oxygen atom of the second water molecule. It is interesting that this spike is absent in $g^{\mathrm{II}}_{e\mathrm{O}}(r)$ indicating that the second water molecule plays a weaker role in the localization process. The weaker localization seen in $g^{\mathrm{II}}_{e\mathrm{O}}(r)$ is also consistent with the higher barrier and lower well depth present in $U^{\mathrm{II}}(\mathbf{r},\mathbf{R}_i)$ when compared to $U^{\mathrm{I}}(\mathbf{r},\mathbf{R}_i)$.

In order to gain insight into the geometry of the system we present an instantaneous snapshot of the isomorphic classical system in Fig. 3. This figure shows that the electron is in a diffuse cloud with an approximate spatial extension of 100 Å. Detailed analysis shows that the electron density is more closely located around one of the water molecules. It can be noticed by inspecting this plot that the tightly bound water dimer is located on the fringe of the electron cloud. Figure 3 and the radius of the gyration projected along the principle axis demonstrate the anisotropy of the electron distribution in this system. In addition a plot of the coordinate of the isomorphic electron–water dimer system projected into the *xy*, *zy*, *xz* planes is displayed in Fig. 4. This figure clearly shows that the two water molecules are located on the fringes of the electron cloud. Both these figures graphically illustrate that the electron is in a diffuse state and the electron density is anisotropically distributed around the water dimer.

Because of the very small binding energy, the effect of electron attachment on the structure of the water dimer is expected to be small. This is born out in our calculation of the pair correlation functions $g_{\mathrm{OH}}(r)$, $g_{\mathrm{OO}}(r)$, and $g_{\mathrm{HH}}(r)$ in the presence of the electron. The only noticeable difference is seen in $g_{\mathrm{HH}}(r)$ which is shown in Fig. (5). The solid (—) and the dash–dot–dash (– · –) curves correspond to the classical $g_{\mathrm{HH}}(r)$ of the neutral water dimer and to that of the water dimer in the presence of the electron, respectively, while the dash–dash (– –) and the dotted lines are the $g_{\mathrm{HH}}(r)$ curves for the corresponding quantum systems. The first thing to observe is that both in the classical and quantal systems there is only a slight increase in some peaks in the presence of the excess electron. There is however a dramatic difference between the quantum $g^{Q}_{\mathrm{HH}}(r)$ and the classical $g^{C}_{\mathrm{HH}}(r)$. The classical water dimer seems to have frozen into two structurally distinct dimer conformations. One of these corresponds to the minimum energy configuration of the classical dimer while the other is obtained by displacing the hydrogen in the hydrogen bond from the O–O axis. Unlike the calculations at 100 K reported elsewhere[26] the dimer is clearly frozen into these configurations. The quantum pair correlation functions is much more diffuse. There is appreciable tunneling into the classically forbidden region and unlike $g^{C}_{\mathrm{HH}}(r)$ the quantum distribution function does not show two distinct structural configurations. Although there

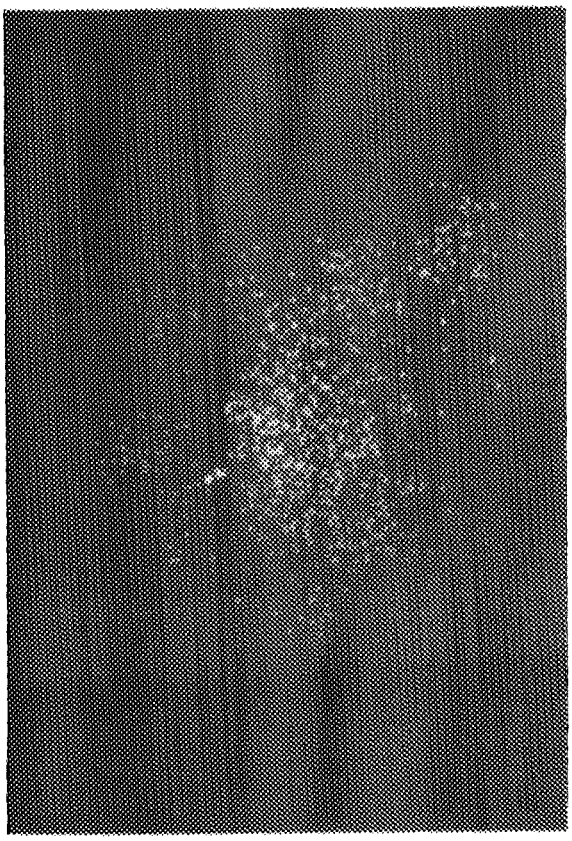

FIG. 3. An instantaneous photograph of the coordinates of the isomorphic electron–water dimer system. The number of beads in the electron chain $P_e = 1000$, whereas the $P_{\mathrm{H,O}} = 100$.

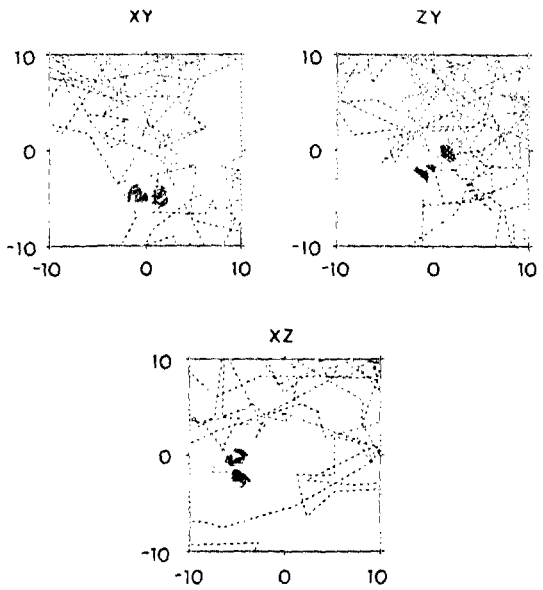

FIG. 4. This figure shows the instantaneous projection of the coordinates of the bound electron–water dimer system onto the *xy*, *zy*, *xz* planes. The coordinates of the isomorphic electron polymer chain are connected by dotted lines. The coordinates of the water molecules are connected by the dark lines. The electron polymer chain is highly diffuse, whereas the water molecules are very localized.

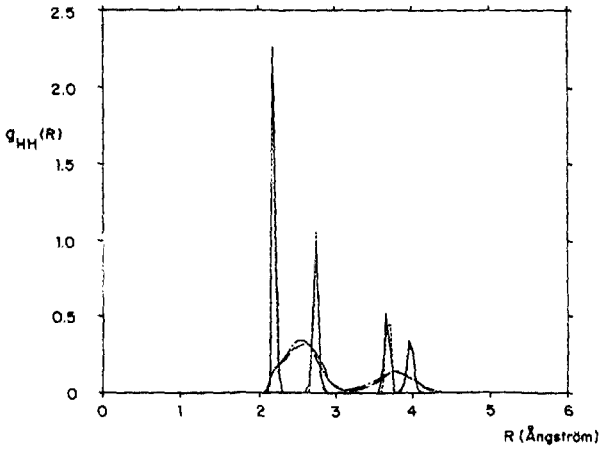

FIG. 5. The hydrogen–hydrogen pair correlation function $g_{HH}(r)$ as a function of r for the neutral water dimer system and the electron–water dimer system. The solid curve and the long dash correspond to $g_{HH}(r)$ for the classical and the quantum neutral water dimer, respectively. The short dash curve represents $g_{HH}(r)$ for the electron–water dimer when the water molecules are treated classically and the dash–dot curve denotes $g_{HH}(r)$ when the water molecules in the electron–dimer system are treated quantum mechanically.

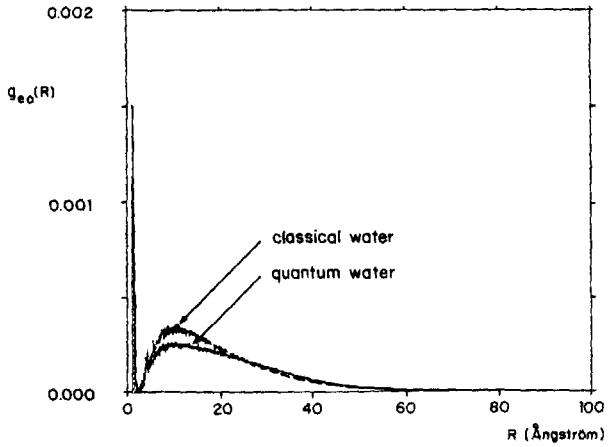

FIG. 6. This figure shows the electron–oxygen pair correlation function, $g_{eO}(r)$, for the electron–water dimer system. The long dashed curve is obtained by treating the water molecules classically and the solid line is calculated by treating the water molecules quantum mechanically. Both the curves were obtained using $U^1(\mathbf{r},\mathbf{R}_i)$.

is a slight increase in the first peak of $g^Q_{HH}(r)$ due to the excess electron there is no appreciable rearrangement in the structure of the water dimer in the presence of the electron. It is interesting to note that Chipman also observed that the excess electron induces insignificant changes in the properties of the water dimer. Although not shown here, our calculations also indicate that both $g_{OH}(r)$ and $g_{OO}(r)$ in the presence of the excess electron look essentially the same as they do in the neutral quantum dimer. Another quantity that shows negligible change in the presence of the electron is the vector sum of the dipole moment of the water dimer. It is found that the dipole moment of the water dimer increases by about 4% when the electron is attached. In Table I it can be seen that when the water molecules are treated quantum mechanically the intermolecular interaction energy is the same both in the presence and in the absence of the electron. There is, however, a substantial difference between the classical and quantum dimer energy. Thus the changes in the intermolecular energy is attributable solely to quantization of the degrees of freedom of the water molecules and is not due to the excess electron. The detailed comparison between the various properties of the water dimer in the presence of the electron and those of the neutral water molecule clearly suggests that the excess electron has a very minor effect on the water dimer. This of course is completely consistent with the notion of very weak binding and a diffuse state.

In Fig. 6 the electron–oxygen radial distribution functions obtained by treating the water quantum mechanically and classically are plotted as a function of r. Both of these curves exhibit a build up of electron density at $r \sim 10$ Å and this is followed by a slowly decaying tail. However $g_{eO}(r)$ corresponding to the classical treatment of the water molecule has a more pronounced peak and decays faster than $g_{eO}(r)$ obtained by treating the water quantum mechanically. The classical water dimer seems to localize the excess electron more strongly than does the quantum water dimer.

TABLE I. Cluster energies[a] at 5 K.

	Intermolecular interaction $V_{H_2O\text{-}H_2O}$		Kinetic energy T	
Configuration	Anion	Neutral	Anion	Neutral
Monomer				
Classical	...	...		0.045
Dimer				
Classical	-2.88 ± 0.01	-2.90 ± 0.01	0.35 ± 0.30	0.090
Quantum	-2.43 ± 0.07	-2.43 ± 0.07	3.98 ± 0.38	3.80 ± 0.40
Trimer SDL				
Classical	-4.02 ± 0.03	-4.03 ± 0.03	0.92 ± 0.12	0.135
Quantum	-3.52 ± 0.06	-3.54 ± 0.06	6.26 ± 0.48	7.65 ± 0.40
Trimer SDC				
Classical	-5.23 ± 0.03	-5.23 ± 0.03		0.135
Quantum	-4.27 ± 0.06	-4.27 ± 0.06		6.74 ± 0.50

[a] All energies reported in kcal/mol.

This is because the quantum dispersion allows the oxygen atoms to penetrate regions which are classically inaccessible. Thus the $g_{eO}(r)$ obtained by treating the dimer quantum mechanically is broader and has less structure. In general one would expect localization to become weaker when the entire system is treated quantum mechanically and this is borne out in Fig. 5.

In light of these calculations, what can one say about the existence of a stable electron–water dimer found in beam experiments?[19] Unfortunately the beam temperature is not known. Accordingly we repeated these calculations at 20 K and the results clearly indicate that the excess electron does not bind to the dimer. This is consistent with the low binding energy already mentioned. Thus these calculations explain the mechanism of the formation of stable electron–water dimer in a molecular beam only if the beam temperature is very low. It is possible that the stability of e^-–$(H_2O)_n$ observed in recent experiments[19] is dynamic in origin. We note that the *ab initio* calculations of Rao and Kestner[16] on larger clusters with fixed cluster geometry also lead to similar conclusions regarding stable cluster formation in molecular beam experiments.

C. Electron–water trimer

The water trimer can exist in different conformations classified by the number of hydrogens of the central molecule that participate in hydrogen bonding. To investigate the nature of binding of an excess electron to a water trimer we confine ourselves to two such configurations. Following Reimers and Watts[25] classification scheme, we label them as the single donor linear (SDL) conformer and the single donor cyclic (SDC) conformer. In the SDL conformation one of the hydrogens of the central molecule is engaged in hydrogen bonding whereas the hydrogens of the two terminal molecules are free. This clearly results in an open linear configuration. In the SDC conformer all three oxygen atoms are essentially equivalent and each molecule has one proton involved in hydrogen bonding. Thus it comes as no surprise that the quantum SDC conformer is more stable than the SDL conformer and this has been explicitly verified by Wallqvist and Berne.[26] However, it is anticipated that at sufficiently low temperatures tunneling effects can give rise to a finite transition rate from one conformer to the other.

We now consider electron attachment to the SDC conformer. In order to assess the possibility of localization we treated the water classically and the number of beads in the electron chain was set equal to 1000. After the system equilibrated various quantities were calculated by averaging over a subsequent 5000 passes. The binding energy was found to be essentially zero indicating that the water trimer in the SDC configuration does not localize the electron. Examination of the configurations of the system clearly indicated that there is no electron density in the field of the trimer moiety. Furthermore the electron chain seemed to physically separate from the water trimer. It has been our experience that in systems which are unbound the acceptance ratios are not stable and this was indeed found to be the case for the solute molecular moves. We also found that these conclusions did not depend on the starting configurations or the step sizes used in the simulation. If the localization is essentially caused by the dipole field of the trimer moiety we expect that no bound state will form because the net vector sum dipole moment of the SDC water trimer is found to be 0.05 D, a value much less than the critical value needed to induce bonding of the electron. Needless to say, the structure of the water trimer as measured by the radial distribution functions $g_{OO}(r)$, $g_{OH}(r)$, $g_{HH}(r)$ remains unchanged when compared to the neutral trimer. We did not test the effect due to neglect of quantum effects in the water molecules on the nature of binding of the electron to the SDC conformer. The treatment of water molecules quantum mechanically is expected to increase the energies and therefore will not qualitatively alter any of the conclusions regarding the attachment of the excess electron.

We now turn to the binding of the electron to the SDL conformer. As before a calculation was done by treating the three water molecules classically and letting the number of beads in the electron chain be 1000. Contrary to the previous study it was found that the classical trimer in the SDL conformer does indeed bind the excess electron with the binding energy of 10.8 meV. This was obtained by averaging over 10 000 passes. In order to assess the importance of treating the water molecules quantum mechanically the number of beads of each of the atoms in a water molecule was increased to 100. This was done in two different ways. In one of the calculations the number of beads in the water molecule in the classically equilibrated system was increased to 100 and in another calculation the system was prepared with $P_{H_2O} = 100$ and $P_e = 1000$ and the system was subsequently equilibrated. Both these calculations yield identical results verifying that the results are independent of the starting configuration. These calculations reveal that the binding energy is between 4–9 meV which is lower than is the case when the water molecules are treated classically. Our calculations also reveal that the dipole moment of the water trimer in the SDL conformer is 2.0 D and this is larger than the critical value of μ required to bind an electron.[31] In Fig. 7 we plot the elec-

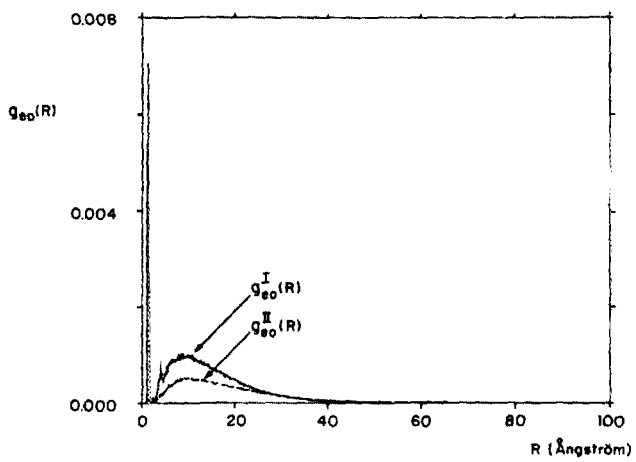

FIG. 7. Plot of the electron–oxygen radial distribution function for the electron–water trimer system. The water trimer is in the single donor linear (SDL) configuration. The solid line denotes $g^{I}_{eO}(r)$ while the dotted line corresponds to $g^{II}_{eO}(r)$.

tron–oxygen radial distribution functions $g^{I}_{eO}(r)$ and $g^{II}_{eO}(r)$ calculated using model potentials $U^{I}(\mathbf{r},\mathbf{R}_i)$ and $U^{II}(\mathbf{r},\mathbf{R}_i)$, respectively. The solid line representing $g^{I}_{eO}(r)$ shows that for $r < 1$ Å there are two sharp closely spaced peaks and this corresponds to the presence of low electron density trapped in the double minima of the potential $U^{I}(\mathbf{r},\mathbf{R}_i)$. There is also a peak in $g^{I}_{eO}(r)$ at $r \sim 4$ Å corresponding to the oxygen atom of the second water molecule. It is clear that there is a substantial peak in $g^{I}_{eO}(r)$ at $r \sim 10$ Å followed by a slowly decaying tail that eventually vanishes at $r \sim 40$ Å. The dashed line denoting $g^{II}_{eO}(r)$ also shows a peak at $r \sim 10$ Å but the range is longer. There is a dramatic decrease in the peak height at $r \sim 10$ Å in $g^{II}_{eO}(r)$ as compared to the one in $g^{I}_{eO}(r)$. This is clearly an indication that the polarizability term plays a key role in enhancing the strength of the binding of the electron by the SDL trimer molecule. Both $g^{I}_{eO}(r)$ and $g^{II}_{eO}(r)$ exhibit a slowly decaying tail indicating that the electron is not strongly localized. The slow decay of $g_{eO}(r)$ suggests that the electron is in a very diffuse state. It is interesting to note that the $g_{eO}(r)$ for the electron–water dimer system is longer ranged than that for the electron–water trimer system (see Fig. 2 for comparison) indicating that the electron is more strongly bound by the SDL water trimer than by the water dimer. This is consistent with the higher binding energy for the electron–trimer system compared to the electron–dimer system.

Because the $g_{eO}(r)$ only represents angularly averaged quantity it is of interest to look for evidence of the anisotropy in the electron density distribution. We have done this by making instantaneous snapshots of the configuration of the system and by projecting the coordinates of the system onto the *xy*, *zy*, *xz* planes. The instantaneous snapshot, shown in Fig. 8, and the projection of the coordinates of the system onto the planes, shown in Fig. 9, both demonstrate that the water molecules are confined to a small volume in space whereas the electron is spatially extended. These figures clearly demonstrate the anisotropy in the electron distribution and also allow one to unequivocally infer that the electron is in a diffuse state.

The electron seems to cause a small but noticeable difference in the trimer structure and this can be seen in Fig. 10 which shows a plot of $g_{HH}(r)$. The solid line corresponds to

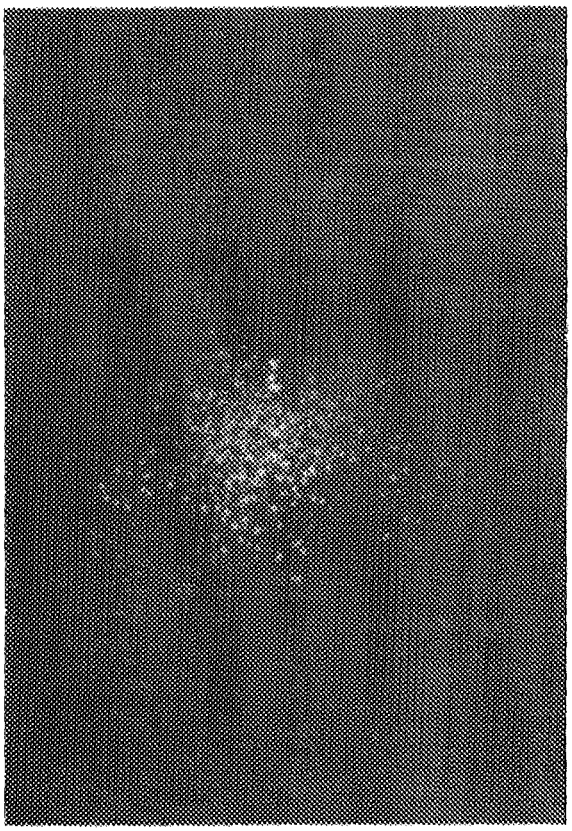

FIG. 8. Instantaneous photograph of the coordinates of the isomorphic electron–water trimer system (with the water in the SDL configuration). The number of beads in the electron chain $P_e = 1000$, whereas $P_{H,O} = 100$.

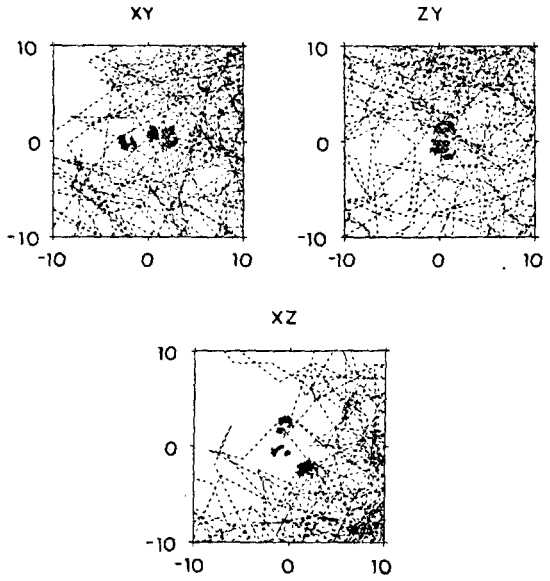

FIG. 9. Projection of the coordinates of the isomorphic electron–water trimer system onto the *xy*, *zy*, *xz* planes. (See caption to Fig. 4.)

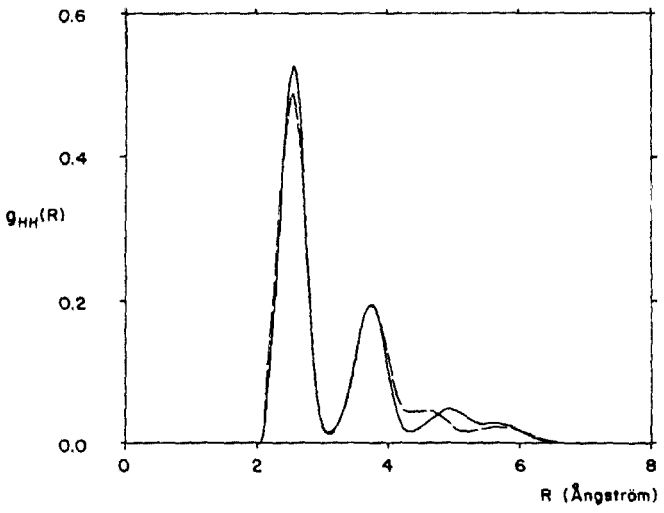

FIG. 10. This figure shows the hydrogen–hydrogen radial distribution function $g_{HH}(r)$ for the neutral water trimer (indicated by the solid line) and for the electron–trimer system (indicated by the dotted line). In both the cases the SDL water trimer is treated quantum mechanically.

$g_{HH}(r)$ of the neutral water SDL trimer, whereas the dash–dash line represents $g_{HH}(r)$ in the presence of the electron. This figure suggests that the electron seems to force the distant hydrogen atoms closer together. As was the case for the dimer there is a significant difference between the structure of the quantum $g_{HH}(r)$ and that of the classical $g_{HH}(r)$ at this temperature. In Table I it can be seen that the intermolecular interaction energy has undergone no change due to electron attachment. There is of course a change in the energy between the classical and quantum SDL trimers with the classical trimer being more stable by about 0.50 kcal/mol.

The results of our calculation show that the electron trimer system is stable when the trimer is in the SDL configuration and this should be detectable in molecular beam experiments. This can also be more clearly demonstrated on energetic considerations as follows. The neutral quantum SDC conformer is about 31 meV more stable than the neutral SDL conformer. Since the binding energy of the electron–SDL system can be as high as 10 meV it follows that these are of comparable stability. Our calculations suggest that an electron will not bind to a preformed SDC conformer. Thus if one can prepare sufficient population of SDL conformer then one should be able to observe binding of an electron to a water trimer in beam experiments. The lack of a e^-–$(H_2O)_3$ peak in the recent beam experiments[20] suggests that the predominant trimer conformer is the SDC one. However, Haberland *et al.*[20] note that when the beam was seeded with Xe instead of Ar they were able to detect weak signals corresponding to e^-–$(H_2O)_3$ system. This suggests that Xe may facilitate the formation of the trimer in the SDL configuration. It would be desirable to perform further experiments to confirm our prediction that if SDL trimer conformer can be formed the resultant anion is more stable than the dimer anion. A SCF calculation for the SDL geometry generated here will also be useful in enhancing our understanding of electron localization in these systems.

IV. CONCLUSIONS

In this paper, we have explored the possibility of electron localization in water clusters using path integral Monte Carlo methods. The major conclusions of our study are:

(a) A single water molecule in its equilibrium geometry does not bind an excess electron.

(b) It is shown that two water molecules can bind an electron. The excess electron is in a spatially diffuse state with binding energy between 3–6 meV. The attached electron does not induce major structural changes in the water dimer, an observation which is consistent with the weak binding energy. These results are in accord with the LCAO-MO-SCF calculations of Chipman.[14,15]

(c) There seems to be a non-negligible difference between the electron oxygen radial distribution function, $g_{eO}(r)$, obtained by treating the water molecules classically and that obtained by treating them quantum mechanically. It is found that a classical water dimer tends to localize the electron more strongly than the quantum water dimer.

(d) The inclusion of the spherical polarizability term enhances the strength of localization and gives rise to larger binding energy.

(e) A trimer molecule in the single donor cyclic conformation does not bind an excess electron. On the other hand, the single donor linear conformer localizes (binds) the excess electron and the binding energy is estimated to be between 4–9 meV. As in the case of the electron–dimer system, the electron is in a diffuse surface state. In contrast to the dimer case the excess electron induces small structural changes in the water trimer with the largest difference being manifested in $g_{HH}(r)$.

(f) One can predict the stability of the e^-–$(H_2O)_n$ system for any n based on dipole arguments alone. However to describe the nature of electron states [as measured by $g_{eO}(r)$] one has to include the polarization term in the e–water potential. This is likely to be important in the case of electron solvation in liquid water.

(g) Given that the potentials we have devised seem reasonable it is of interest to solve the one-body Schrödinger equation for a constrained water geometry to obtain the ground state energy for comparison. In fact this can be done for clusters of any size as long as the geometry of the cluster is fixed. This work is in progress and the results will be reported in a future paper.

The present calculations suggest that the model potentials employed here for the electron–water interactions may indeed be reasonable. We are presently extending these calculations to explore the nature of localization of an electron in larger water clusters. In addition we are using these and other model potentials to characterize the structure and energetics of the solvated electron[22] in bulk water.

ACKNOWLEDGMENT

The authors are grateful to John E. Straub for assistance in taking the photographs.

[1] *The Hydrated Electron*, edited by E. J. Hart and M. Anbar (Wiley, New York, 1970); *Metal Ammonia Solutions*, edited by J. J. Lagoski and M. J. Sienko (Butterworths, London, 1970); E. A. Cotterell and N. F. Mott, Adv. Phys. **18**, 665 1969; M. H. Cohen and J. C. Thompson, *ibid.* **17**, 85 (1968).
[2] G. A. Kenney Wallace, Acc. Chem. Res. **11**, 433 (1978); S. A. Rice, *ibid.* **1**, 181 (1968).
[3] *Electrons in Fluids*, edited by J. Jortner and N. R. Kestner (Springer, New York, 1973).
[4] A. M. Brodsky and A. R. Tsaversky, Adv. Chem. Phys. **44**, 483 (1980).
[5] For a classification of these excess electron states, see J. Jortner and A. Gaathon, Can. J. Chem. **55**, 1801 (1977).
[6] For a review of the behavior of an electron in nonpolar solvents, see H. T. Davis and R. G. Davis, Adv. Chem. Phys. **31**, 329 (1975).
[7] M. Parrinello and A. Rahman, J. Chem. Phys. **80**, 860 (1984); J. Bartholomew, R. W. Hall, and B. J. Berne, Phys. Rev. B **32**, 548 (1985).
[8] U. Landman, D. Scharf, and J. Jortner, Phys. Rev. Lett. **54**, 1860 (1985).
[9] N. F. Mott and E. A. Anderson, *Electronic Processes in Non-Crystalline Materials* (Clarendon, Oxford, 1971); N. F. Mott, J. Phys. Chem. **79**, 2915 (1975); For a discussion of the current theories of an electron in disordered media and its role in the metal insulator transition, see P. A. Lee and T. V. Ramakrishnan, Rev. Mod. Phys. **57**, 287 (1985).
[10] (a) D. Chandler, Y. Singh, and D. M. Richardson, J. Chem. Phys. **81**, 1975 (1984); (b) A. L. Nichols III, D. Chandler, Y. Singh, and D. M.

Richardson, *ibid.* **84**, 398 (1986).
[11]K. Fueki, D. F. Feng, and L. Kevan, J. Am. Chem. Soc. **95**, 1398 (1975); D. A. Copeland, N. R. Kestner, and J. Jortner, J. Chem. Phys. **53**, 189 (1970).
[12]K. Iguchi, J. Chem. Phys. **48**, 1735 (1968); **51**, 3137 (1964); N. R. Kestner, Can. J. Chem. **55**, 1937 (1977).
[13]M. Newton, J. Phys. Chem. **79**, 2795 (1975).
[14]D. Chipman, J. Phys. Chem. **82**, 1980 (1978).
[15]D. Chipman, J. Phys. Chem. **83**, 1657 (1979).
[16]N. R. Kestner and J. Jortner, J. Phys. Chem. **88**, 3818 (1984).
[17]B. K. Rao and N. R. Kestner, J. Chem. Phys. **80**, 3818 (1984).
[18]J. Jortner, Ber. Bunsenges, Chem. **88**, 188 (1984).
[19]H. Haberland, H. G. Schindler, and D. R. Worsnop, Ber. Bunsenges, Chem. **88**, 270 (1984); J. Phys. Chem. **88**, 3903 (1984).
[20]H. Haberland, C. Lindewight, H. G. Schindler, and D. R. Worsnop, J. Chem. Phys. **81**, 3742 (1984).
[21]See the footnote (7) in Ref. 16, indicating the futile attempts by R. Compton (Oak Ridge) and D. Herschbach and E. Quepevis to find negatively charged water clusters in charge exchange experiments.
[22]A. Wallqvist, D. Thirumalai, C. Pangali, and B. J. Berne (manuscript in preparation).
[23]C. D. Jonah, C. Romero, and A. Rahman, Chem. Phys. Lett. **123**, 209 (1986); P. J. Rossky, J. Schnitker, and R. A. Kuharski, J. Stat. Phys. (to be published).
[24]H. L. Lemberg and F. H. Stillinger, J. Chem. Phys. **62**, 1677 (1975); A. Rahman, R. H. Stillinger, and H. L. Lemberg, *ibid.* **63**, 5223 (1975); F. H. Stillinger and A. Rahman, *ibid.* **68**, 666 (1978).
[25]J. R. Reimers and R. O. Watts, Chem. Phys. Lett. **94**, 222 (1982); Chem. Phys. **85**, 83 (1984); Mol. Phys. **52**, 357 (1984). Note that in these papers the dimensionless coordinate S_3 is everywhere erroneously defined as being twice as large as it should be.
[26]A. Wallqvist and B. J. Berne, Chem. Phys. Lett. **117**, 214 (1985).
[27]L. R. Kahn, R. Baybutt, and D. G. Truhlar, J. Chem. Phys. **65**, 3826 (1976).
[28]The experimental value for the dipole moment was used and the spherical polarizability was taken from H. J. Werner and W. Meyer, Mol. Phys. **31**, 855 (1976).
[29]C. H. Douglas, D. A. Weil, P. A. Charles, R. A. Eades, D. G. Truhlar, and D. A. Dixon, in *Chemical Applications of Atomic and Molecular Potentials,* edited by P. Politzer and D. G. Truhlar (Plenum, New York, 1981).
[30]For the use of this isomorphism in the chemical physics context, see D. Chandler and P. G. Wolynes, J. Chem. Phys. **74**, 4078 (1981); D. Thirumalai, R. W. Hall, and B. J. Berne, *ibid.* **81**, 2523 (1984); R. Kuharski and P. J. Rossky, *ibid.* **82**, 5164 (1985); B. De Raedt, M. Sprik, and M. L. Klein, *ibid.* **80**, 5719 (1984).
[31]W. R. Garrett, J. Chem. Phys. **73**, 5721 (1980); **77**, 3666 (1982).